scientific reports

Check for updates

OPEN

Mechanistic insights into the Japanese encephalitis virus RNA dependent RNA polymerase protein inhibition by bioflavonoids from *Azadirachta indica*

Vivek Dhar Dwivedi[1], Ankita Singh[2], Sherif Aly El-Kafraway[3,4], Thamir A. Alandijany[3,4], Arwa A. Faizo[3,4], Leena Hussein Bajrai[3,5], Mohammad Amjad Kamal[3,6,7] & Esam Ibraheem Azhar[3,4]✉

Japanese encephalitis (JE) virus is a flavivirus causing encephalitis causing neurological damage. RNA-dependent-RNA-polymerase (RdRp) is responsible for genome replication making it excellent anti-viral target. In this study, the crystal structure of JE RdRp (jRdRp) and bioflavonoids reported in *Azadirachta indica* were retrieved from specific databases. Structure-based virtual screening was employed using MTiOpenScreen server and top four compounds selected with the most negative docking scores. Conformations were redocked using AutoDock Vina; these complexes showed mechanistic interactions with Arg^{474}, Gly^{605}, Asp^{668}, and Trp^{800} residues in the active site of jRdRp, i.e., guanosine-5′-triphosphate. Furthermore, 100 ns classical molecular dynamics simulation and binding free energy calculation showed stability of docked bioflavonoids in the active jRdRp pocket and significant contribution of van-der-Waals interactions for docked complex stability during simulation. Therefore, this study predicted the anti-viral activity of Gedunin, Nimbolide, Ohchinin acetate, and Kulactone against jRdRp and can be considered for further antiviral drug development.

Japanese encephalitis (JE), a serious vector-borne viral infection caused by the Japanese encephalitis virus (JEV), is responsible for causing Epidemic encephalitis B—an acute infectious disease of the central nervous system, in 24 countries of Southeast Asia and the Western Pacific[1–3]. As the transmission of JE is highly dynamic, several studies have reported substantial variation in the estimation of its global impact. For instance, a comprehensive survey estimated more than 69,000 cases per year of JE in the past decade, but other estimates drastically differ incidences—from 50,000 to 175,000 cases per year[4–7]. About 30–50% of JE survivors have been documented with permanent neurological sequelae, imposing a heavy burden on public health and society[6,8]. Also, a worldwide influence from JE in 2002 was estimated as 709,000 disability-adjusted life years annually[7], advised it the one of the critical arboviral infection in humans[2].

The positive-sense, single-stranded RNA Japanese encephalitis virus (JEV) belongs to genus *Flavivirus*, family Flaviviridae, and has ~ 50 nm icosahedral-shaped lipoprotein capsid, which encapsulates a 11 kb RNA genome embedded with core protein[9]. Viral genome sequence includes 5′ and 3′ untranslated regions and a single open reading frame (ORF) with no poly(A) tail, which translates into unsegmented polyprotein of 3432 amino acids—it further sliced and processed into three structural and seven nonstructural proteins[10–12]. Herein, the N-terminal of the polyprotein translates for the structural proteins [capsid protein (C), membrane M protein (PrM), and

[1]Centre for Bioinformatics, Computational and Systems Biology, Pathfinder Research and Training Foundation, Greater Noida 201308, India. [2]School of Environmental Sciences, Jawaharlal Nehru University, New Delhi 110067, India. [3]Special Infectious Agents Unit, King Fahd Medical Research Center, King Abdulaziz University, Jeddah, Saudi Arabia. [4]Department of Medical Laboratory Technology, Faculty of Applied Medical Sciences, King Abdulaziz University, Jeddah, Saudi Arabia. [5]Biochemistry Department, Faculty of Sciences, King Abdulaziz University, Jeddah, Saudi Arabia. [6]Enzymoics, Novel Global Community Educational Foundation, 7 Peterlee Place, Hebersham, NSW 2770, Australia. [7]West China School of Nursing/Institutes for Systems Genetics, Frontiers Science Center for Disease-Related Molecular Network, West China Hospital, Sichuan University, Chengdu 610041, Sichuan, China. ✉email: eazhar@kau.edu.sa

envelope protein (E)], while the non-structural (NS) proteins (NS1, NS2A, NS2B, NS3, NS4A, NS4B, and NS5) are encoded by the C-terminal of the polyprotein. This maturation procedure utilizes both the viral and host proteases[2]. Later, the seven NS proteins coordinate to form complex machinery regulating replication, cleavage of polyprotein, and fabrication of nascent viral particles[13–15]. Among these NS protein, NS5 is the largest and the most conserved protein of the JEV which comprises an N-terminal *S*-adenosyl-L-methionine (SAM)-dependent methyltransferase (MTase) domain and a C-terminal RNA-dependent RNA polymerase (RdRp) region[12,16]. The RdRp in cooperation with other NS proteins and host cell proteins participates in the viral genome synthesis by forming a membrane-bound replication complex (RC)[17–20]. Replication process of viral genome involves the synthesis of complimentary negative RNA strand from the positive-sense single-strand RNA, which acts as a template to form double-stranded replicative form (RF). The negative strand of RF is then used as a template to produce large copies of positive strand RNA which further acts as a genomic RNA after the release from replicative intermediate (RI). The indispensable nature of RdRp in RNA synthesis for viral replication and absence of homologous protein in humans makes it a favourite target molecule for anti-viral drugs.

JEV is mainly transmitted by the mosquito *Culex tritaeniorrhynchus* in endemic regions, which prefers to breed in irrigated rice paddies[6], making *Culex* a primary host and reservoir to complete its sylvatic life cycle[21]. Besides, it was predicted to maintained in an enzootic cycle in pigs and wild birds in which humans are dead-end hosts[4]. In humans, as a neurotropic virus, it can cross blood–brain barrier (BBB) and replicate in Purkinje cells, granule cells, and pyramidal neurons of cerebrum causing a wide array of neurological complications, including acute encephalitis[22–25]. JEV infection is more common in young children but can also infect the adults and majority of the cases shows mild or no symptoms[26,27]. Severe clinical illness is characterized by high fever, headache, vomiting, neck stiffness, disorientation, coma, seizures, spastic paralysis, and aseptic meningitis or encephalitis[2,28]. Although vaccines have reduced the morbidity and mortality from the infection and the multiple reports of compounds showing activities against JEV infection, such as *N*-nonyl-deoxynojirimycin[29], Dehydroepiandrosterone[30], *N*-methylisatin-beta-thiosemicarbazone derivative (SCH 16)[31], Indirubin[32], Manidipine[33], Chlorpromazine[34], Etanercept[35], Minocycline[36], Ouabain and Digoxin[37], only few drugs are in use to treat patients with JEV are available.

To deliver the urgent need for anti-JEV therapy, traditional knowledge has long been used at the community level to limit the clinical manifestations; and hence, warrants the molecular exploration of potential novel molecules. For example, screening of natural extracts against JEV infection resulted in the identification of two natural compounds, i.e., Ouabain and Digoxin[37]. *Azadirachta indica* (Neem) of family Meliaceae is one such valuable traditional knowledge-based plant that exhibits medicinal properties like anticancer, anti-inflammatory, antidiabetic, antibacterial, antifungal, antimalarial, antiviral, etc.[38]. Of note, compounds from various parts of the neem together with leaves, seeds, fruits, flowers, bark, and roots are widely used in humans because of their antimicrobial and antiviral properties[39–42]. For instance, flavonoids from neem extracts were reported for significant inhibition of the Dengue virus type 2[43]. Considering the wealth of traditional knowledge and advancements in computer-aided drug discovery, we employed virtual high-throughput screening approach to screen 43 biological active bioflavonoids from neem plant against jRdRp protein. Following potential ligands were studied for binding stabilities and affinities using molecular simulations and free energy calculations, respectively to understand the detailed mechanistic mechanism and other characteristics involved in the RdRp inhibition of JEV.

Materials and methods

Virtual screening and ADMET predictions. Crystal Structure of viral Japanese encephalitis virus RNA dependent RNA polymerase (jRdRp) protein in complex with guanosine-5′-triphosphate (GTP) (PDB ID: 4HDG)[44] solved at 2.38 Å resolution was used as the receptor molecule for structure based virtual screening with the natural compounds from neem plant (*Azadirachta indica*) at MTi-OpenScreen webserver[45]. Herein, a total of 43 bioactive bioflavonoids reported in *Azadirachta indica* were searched in the literature and their 3D conformations were downloaded from the PubChem database (https://pubchem.ncbi.nlm.nih.gov/)[46]. For structure based virtual screening, initially the receptor was processed by following steps: (1) removal of crystalized water molecules and heteroatoms, (2) assignment of Gasteiger charges, (3) addition of polar hydrogen atoms and (4) removal of non-polar hydrogen atoms using default parameters of Dock Prep tool in UCSF Chimera-1.14[47]. Following, collected bioactive compounds were screened at the catalytic site in jRdRp using MTi-OpenScreen webserver. After that, top four bioactive compounds with highest negative docking score were considered for further ADMET (Absorption, distribution, metabolism, excretion, and toxicity) analysis using SwissADME (http://www.swissadme.ch)[48] and AdmetSAR (http://lmmd.ecust.edu.cn/admetsar1/) servers[49].

Re-docking simulation and binding pose profiling. Molecular docking simulation between the jRdRp and potential natural compounds was performed by Chimera-AutoDock Vina plugin setup to decipher the most interacting residues in the active site of jRdRp against reference molecules, as reported earlier[50]. Briefly, 3D structure of protein and potential bioflavonoids as ligand were subjected to minimization under the default parameters in structure minimization tool in UCSF Chimera-1.14[47]. Later, both receptor and ligands were primed for docking in Dock prep tool in Chimera with default parameters, where native ligand from the crystal structure was removed, polar hydrogen atoms hydrogen atoms and charges were added. Finally, molecular docking simulations were performed using AutoDock Vina[51] as plugin under default setting at the nucleotide binding site in jRdRp protein by adjusting the grid size of $30 \times 30 \times 30$ Å along both three (X, Y, and Z) axes, covering all the essential residues centre at − 38.85, − 0.98, − 43.61 Å region, to distribute profuse space to the conformations of ligands during docking processes. Herein, at least 10 docked poses for the ligands were collected and conformation with highest negative docking score and least root mean square deviation (by default 0 in AutoDock Vina) were extracted for further binding pose analysis under default parameters using 2D interaction diagram

in free academic Desmond-maestro 2018.4 52 (Schrödinger Release 2018-4: Desmond Molecular Dynamics System, D. E. Shaw Research, New York, NY, 2018. Maestro-Desmond Interoperability Tools, Schrödinger, New York, NY, 2018). Finally, all the 3D and 2D interaction images were generated in Desmond-maestro 2018.4[52]. Similar docking protocol was used for the natural substrates ATP and GTP as reference molecules for comparative binding pose analysis against selected bioactive compounds.

Classical molecular dynamics simulation. Molecular dynamics simulation method was employed to analyse the stability and intermolecular interactions of the selected protein–ligand complexes obtained from the docking experiments. MD simulations for the docked complexes were performed under Linux environment on HP Z2 Microtower workstation using Desmond-maestro 2018.4[52]. The simulation system was prepared using the system builder module in Desmond and TIP4P model was employed for the solvation of the docked complex by placing in a 10 Å × 10 Å × 10 Å orthorhombic box. Later, the complete system was neutralized by adding Na^+ or Cl^- counter ions to maintain the neutrality and further minimized under default parameters using minimization tool. Finally, the whole system was subjected to simulation at a temperature of 300 K and pressure of 1.01325 bar using Nose–Hoover thermostat and Martyna–Tobias–Klein method, respectively under default parameters. Each system, including reference complex, were simulated for 100 ns under default parameters with OPLS (optimized potentials for liquid simulations)-2005 force field, where a total of 5000 frames were collected at 20 ps interval during the simulation interval using molecular dynamics tool of Desmond-maestro 2018.4[52]. Finally, the generated trajectories were analysed for root-mean-square deviation (RMSD), root-mean-square fluctuation (RMSF), and protein–ligand interaction profiling with the aid of Simulation Interaction Diagram (SID) module of Desmond-maestro 2018.4[52].

Molecular mechanics/generalized born surface area calculation. Following MD simulation of selected protein–ligand complexes, end point based binding free energy method, i.e., Molecular Mechanics-Generalized Born Surface Area (MM/GBSA) was applied to the extracted poses at every 10 ns from each simulation trajectory to calculate the mean binding free energy under default parameters via Prime MMGBSA module of the MM/GBSA protocol in Schrödinger suite (Schrödinger Release 2018.3: Prime, Schrödinger, LLC, New York, NY, 2018). In this method, extracted poses were refined by deletion of solvent molecules and ions, as reported earlier[53]. Finally, net free binding energy (ΔG) was calculated using the following Eq. (1).

$$\Delta G_{\text{bind}} = \Delta G_{\text{complex(minimized)}} - (\Delta G_{\text{receptor(minimized)}} + \Delta G_{\text{ligand(minimized)}}) \quad (1)$$

where ΔG_{bind} denotes the binding free energy, $\mathbf{\Delta G}_{complex,}$ indicates the free energy of the complex, $\mathbf{\Delta G}_{receptor}$ and $\mathbf{\Delta G}_{ligand}$ exhibits the energy for receptor and ligan, respectively.

Results and discussion

Structure based virtual screening. A total of 43 bioflavonoids (Table S1) documented in *Azadirachta indica* were collected from the literature and used in virtual screening against the catalytic site in jRdRp protein. All the compounds showed considerable binding affinity between − 11.6 and − 5.2 kcal/mol with the active residues of viral jRdRp protein (Supplementary Table S1). Following top four compounds, i.e., Gedunin, Nimbolide, Ohchinin acetate, and Kulactone, with higher docking scores were considered for further re-docking and intermolecular interaction analysis against native crystalized ligand, i.e., guanosine-5′-triphosphate (GTP) and Adenosine triphosphate (ATP) as reference molecules (Fig. 1).

ADME profiling. The intrinsic properties, such as drug-likeness and pharmacological characteristics, have been marked as an important factor for compounds under medical applications. Hence, ADMET properties for top four selected compounds, i.e., Gedunin, Nimbolide, Ohchinin acetate, and Kulactone, were predicted using SwissADME and admetSAR, which help to analyse the pharmacokinetic and toxic properties of compounds (Fig. 2, Supplementary Table S2). All four selected bioflavonoids show negative AMES toxicity test and non-carcinogenic profile which reveals the non-mutagenic nature of compounds predicted using admetSAR. Cytochrome P450 2D6 (CYP2D6) is an enzyme plays vital role in the metabolism of drugs and xenobiotics and inhibition of this enzyme can lead to drug-drug interactions. Interestingly, all the selected bioflavonoids were found to be non-inhibitors of CYP2D6 using SwissADME along with other cytochromes; list of the complete ADME (absorption, distribution, metabolism, and excretion) profiling for the selected bioactive compounds is given in Supplementary Table S2. Notably, Gedunin and Nimbolide exhibit high gastrointestinal absorption while Ohchinin acetate and Kulactone show low gastrointestinal absorption, and each of these bioflavonoids exhibit no crossing through Blood Brain Barrier (BBB). Also, Gedunin and Nimbolide shows zero violation of Lipinski`s rule of five; however, Kulactone and Ohchinin acetate shows one violation of Lipinski`s rule of five. Additionally, other four rules for drug likeness, including Ghose, Veber, Egan, and Muegge violations, showed Nimbolide as ideal candidate (Supplementary Table S2). However, it is important to mentioned that rules for drug-likeness are not applicable to the natural bioactive compounds as these agents can be identified by the active transport system of the cells when contemplating "druggable chemical entities"[54,55]. In addition, other properties such as pharmacokinetics and medicinal chemistry friendliness were computed for the potent compounds (Supplementary Table S2). Conclusively, the screened compounds were suggested with ideal medical properties.

Re-docking and intermolecular interaction analysis. Structure based virtual screening algorithms are fast and comparatively less accurate; hence, typically best conformations of the ligands has been suggested to

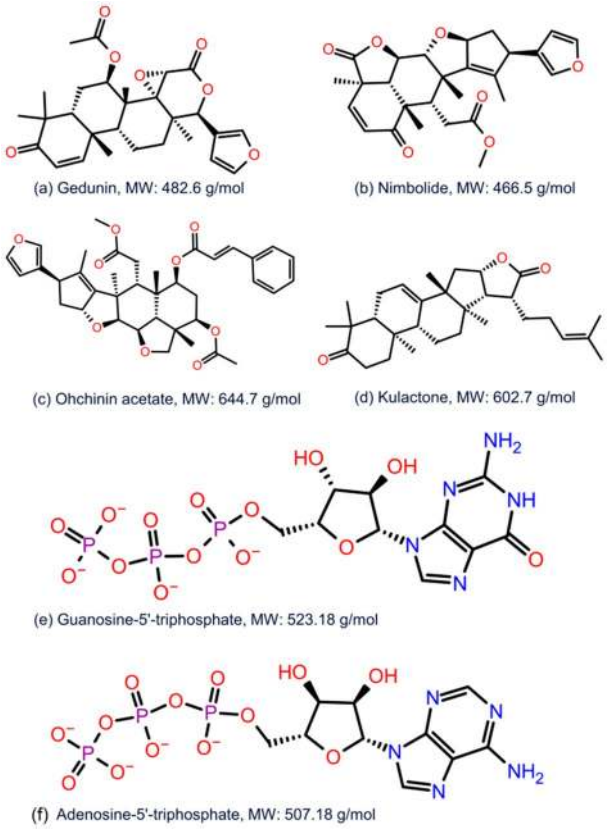

Figure 1. 2D structural formula and molecular weight for the selected bioflavonoids, i.e., (**a**) Gedunin, (**b**) Nimbolide, (**c**) Ohchinin acetate, and (**d**) Kulactone and reference ligand, viz. (**e**) Guanosine-5′-triphosphate (**f**) Adenosine-5′-triphosphate.

consider for re-docking via stringent molecular docking protocols. Thus, re-docking was performed using AutoDock Vina to collect the most suitable binding poses and conformations for the selected bioactive compounds in the active site of jRdRp protein at least docking RMSD (default 0 in AutoDock Vina) values and highest negative docking scores. Interestingly, selected bioactive compounds, i.e., Gedunin, Nimbolide, Ohchinin acetate, and Kulactone exhibit substantial docking scores (> − 10 kcal/mol) against reference molecules (− 9.0 and − 8.6 kcal/mol), viz. GTP and ATP (Supplementary Table S3). These results suggested the considerable binding affinity of bioactive compounds in the active pocket of jRdRp protein.

To understand the mechanistic interactions, each docked pose of bioflavonoids was studied for intermolecular interaction profile by comparison to reference molecules. The docked complex of jRdRp-Gedunin showed − 10.4 kcal/mol docking score and formation of two hydrogen bonds (Ser^{604} and Ile^{802} residues). Additionally, hydrophobic (Leu^{411}, Ala^{413}, Val^{414}, Ala^{475}, Ile^{476}, Trp^{477}, Tyr^{610}, Trp^{800}, and Ile^{802} residues), polar (Ser^{604}, Thr^{609}, Asn^{613}, and Ser^{801} residues), negative (Asp^{541} and Asp^{668} residues), positive (Arg^{474} and Arg^{460} residues), and glycine (Gly^{412}, and Gly^{605} residues) interactions were also noted to contribute for the stability of respective docked complex (Fig. 3a,b). Likewise, docking of Nimbolide with jRdRp protein exhibited − 10.9 kcal/mol docking score and formation of three hydrogen bonds at Ser^{604}, Ser^{801}, and Ile^{802} residues. Also, jRdRp-Nimbolide complex shows additional interactions with essential residues, includes hydrophobic (Leu^{411}, Ala^{413}, Val^{607}, Tyr^{610}, Cys^{714}, Trp^{800}, and Ile^{802}), polar (Ser^{604}, Gln^{606}, Thr^{609}, Asn^{613}, Ser^{666}, Ser^{801}, and His^{803}), negative (Asp^{668} and Asp^{669}), positive (Lys^{404}, Arg^{474}, and Lys^{471}) and glycine (Gly^{412} and Gly^{667}) interactions (Fig. 3c,d). Moreover, jRdRp-Ohchinin complex also presented − 11 kcal/mol docking energy and noted for four hydrogen bonds (Trp^{477}, Ser^{604}, Ser^{801}, and Ile^{802} residues), hydrophobic (Ala^{410}, Leu^{411}, Ala^{413}, Val^{414}, Ala^{475}, Ile^{476}, Trp^{477}, Val^{607}, Tyr^{610}, Cys^{714}, Trp^{800}, and Ile^{802} residues), polar (Asn^{495}, Ser^{604}, Thr^{609}, Asn^{613}, Ser^{801}, and His^{803} residues), negative (Asp^{668} and Asp^{669} residues), positive (Lys^{404}, Arg^{460}, Arg^{474}, and Lys^{47} residues), and glycine (Gly^{412}, Gly^{603}, Gly^{605}, and Gly^{667} residues) interactions, which were predicted to provide complex stability (Fig. 3e,f). Furthermore, only one hydrogen bond was observed in the jRdRp-Kulactone docked complex with − 10.4 kcal/mol docking score and contribution of supplementary interactions with essential residues, such as hydrophobic (Val^{414}, Phe^{415}, Ala^{475}, Ile^{476}, Phe^{478}, Tyr^{610}, and Trp^{800}), polar (Thr^{346}, Ser^{604}, Thr^{609}, Asn^{613}, and Ser^{666}), negative (Asp^{541} and Asp^{668}), positive (Arg^{460} and Arg^{474}), and glycine (Gly^{412}, Gly^{605}, and Gly^{667}) interactions (Fig. 3g,h). Notably, no π-π interactions and salt bridge formation were recorded in the bioactive compounds docked complexes with jRdRp protein (Fig. 3).

Interestingly, the re-docking of GTP as reference molecule in the same active pocket reveals − 9.0 kcal/mol and interactions with key residues, including seven hydrogen bonds formation (Asp^{541} (2), Asp^{668}, Asp^{669}, and Ser^{715}), pi-cation (Arg^{474}), salt bridge formation (Arg^{474}, and Lys^{463} (2)), hydrophobic (Trp^{54}, Tyr^{610}, Cys^{714}, and

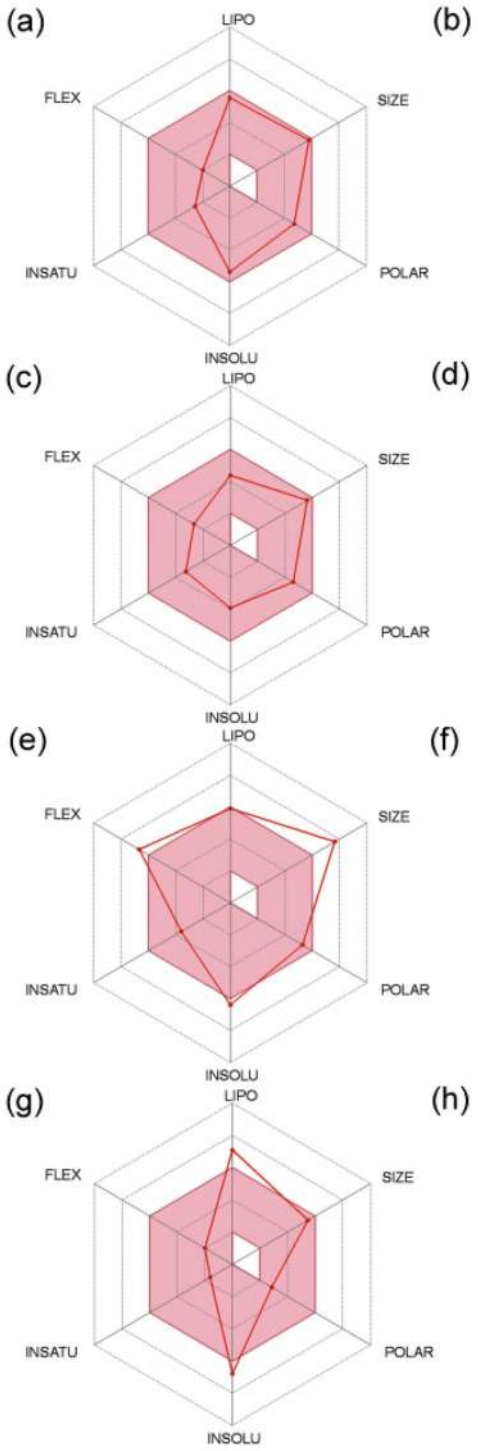

Figure 2. ADMET analysis for the selected bioflavonoids, i.e., (**a**,**b**) Gedunin, (**b**,**c**) Nimbolide, (**d**,**e**) Ohchinin acetate, and (**f**,**g**) Kulactone, as inhibitor against jRdRp.

Ile[802]), polar (Ser[604], Asn[613], Ser[666], Ser[715], Ser[799], Ser[801], and His[803]), negative (Asp[541],Asp[668], and Asp[669]), and positive (Lys[463], Lys[471], Arg[474], and Arg[734]) interactions. In crystal structure, nucleoside moiety of GTP forms hydrogen bonds with Asp541, Ser604, Asp668, and Asp669, and pi-cation interaction with Arg474 while redocked poses showed similar interactions as in crystal structure, except Ser604 which forms polar contact with nucleoside moiety of GTP. (Supplementary Figure S1). Lys463, Arg734, Arg742, and Ser799 residues in active cavity of jeRdRp also formed hydrogen bonds with the phosphate moiety of GTP in the crystal structure.

In re-docking case of ATP as reference molecule in the same active pocket reveals − 8.6 kcal/mol and interactions with key residues, including seven hydrogen bonds formation (Leu[411], Ala[413], Val[607](2), Val[608], Tyr[610], Cys[714] and Ile[802]), hydrophobic (Leu[411], Ala[413], Val[607](2), Val[608], Tyr[610], Cys[714] and Ile[802]), polar (Ser[604], Gln[606],

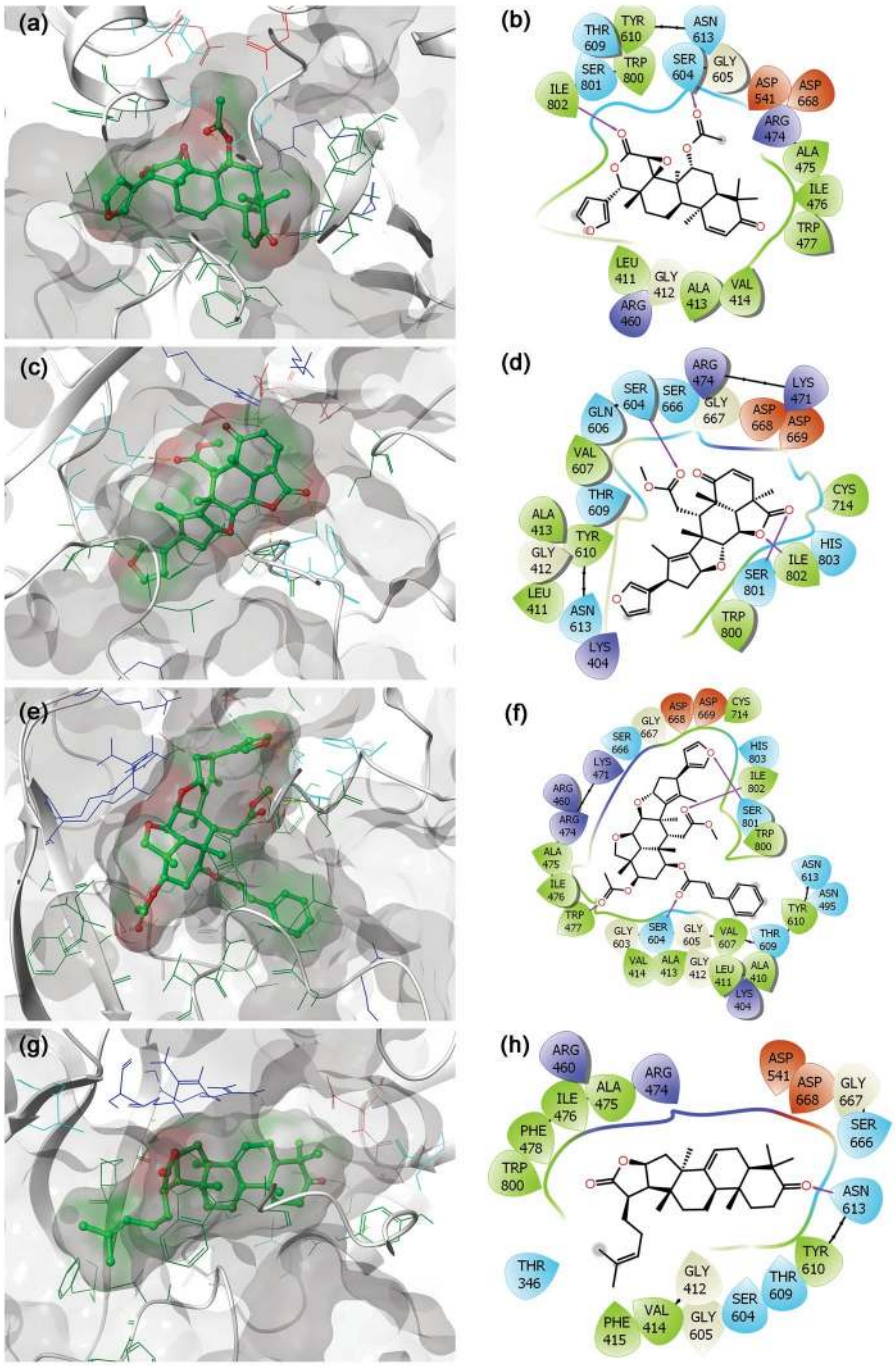

Figure 3. 3D and 2D docked poses of the selective bioflavonoids, i.e., (**a**,**b**) Gedunin, (**c**,**d**) Nimbolide, (**e**,**f**) Ohchinin acetate, and (**g**,**h**) Kulactone, collected at 4 Å space around the ligand within in the active site of jRdRP protein. In 3D structures, protein surface and ligand surface were rendered based on the alpha-carbon and atomic charge, respectively. While in 2D maps, hydrogen bond formation (pink arrows), hydrophobic (green), polar (blue), red (negative), violet (positive), glycine (grey) interactions are logged for docked complexes of jRdRp with selected bioactive compounds.

Thr[609], Asn[613], Ser[715], Ser[801], His[803]), negative (Asp[668], and Asp[669]), positive (Arg[734], Lys[471] and Arg[474]), and glycine (Gly[412] and Gly[667]) interactions (Supplementary Figure S2). In re-docked complexes of reference molecules, the orientation of GTP and ATP was silghty different in their original binding pocket of jRdRp when compared to their crystal structures (Supplementary Figure S3–4). Of note, interacting residues were also noted in the crystal structure of jRdRp-GTP and jRdRp-ATP complex and essentially required to conduct the replication of viral RNA genome[44]. Overall, molecular contact analysis showed interaction of docked bioactive compounds with essential residues of the A, B, C, E and F motifs and the priming loop in viral RdRp protein (Fig. 3, Supplementary

Table S3). Hence, these findings suggested the screened bioactive compounds in the order of Ohchinin acetate, Nimbolide, Gedunin, and Kulactone as potential inhibitors of jRdRp by comparison to reference ligands.

Classical molecular dynamics simulation analysis. In computational drug discovery, molecular dynamics (MD) simulation is used to predict the docked complexes stability and formation of intermolecular interaction in reference to time[56,57]. In this study, the stability of docked complexes was monitored by means of root mean square deviation (RMSD), root square means fluctuation (RMSF), and protein–ligand contact mapping, extracted from respective 100 ns simulation trajectories. Typically, RMSD and RMSF are used to observe the structural fluctuations which are essentially required to establish the dynamic stability of the system. Furthermore, the protein and ligands contact maps are analysed to calculate the intermolecular interaction in docked poses as function of time during simulation interval scrutinize the stability of docked ligands at the active pocket of viral protease.

RMSD and RMSF analysis. Initially, docked complexes of potential bioactive compounds with JRdRp were analyzed for protein and ligand RMSD with respect to initial pose as reference frame (Fig. 4). In all the docked complexes, RMSD for jRdRp showed deviations < 2.8 Å till 60 ns, except JRdRp-Kulactone showed deviations between 4.5 and 5.8 Å till end of the 100 ns simulation interval. However, jRdRp docked with reference ligands, i.e., GTP, exhibits acceptable deviations (~ 1.50 to 2.0 Å) and stability during the simulation interval (Supplementary Figure S5) while docked complex with ATP showed deviations < 3.2 Å till 40 ns followed by variations and a maximum of < 5.6 Å was noted at the end of 100 ns MD simulation interval (Supplementary Figure S6). These observations were further supported by the calculated RMSF values (< 3.5 Å), except higher deviations (< 5–7.2 Å) were noted in the C-terminal of jRdRp protein docked with Nimbolide and Ohchinin acetate. Also, acceptable deviations (< 3.5 Å) were observed in the residues of jRdRp protein interacting with the respective docked ligands (Supplementary Figure S7). Collectively, these observations suggested the considerable rigidity and stability in jRdRp protein docked with bioactive compounds during the simulation without major structural deformations. Besides, docked bioactive compounds, i.e., Gedunin, Nimbolide, Ohchinin acetate, and Kulactone, at the active site of jRdRp protein showed considerable RMSD values till 100 ns with acceptable deviations (< 3–3.8 Å), indicates the stability of docked ligands in the active site of jRdRp protein (Fig. 4). Likewise, reference molecule, viz. GTP, also exhibits acceptable RMSD (< 3 Å) fit at the active site of jRdRp protein revealed the substantial stability of respective docked complex (Supplementary Figure S5). In case of reference molecule ATP, no change in the protein structure was observed while ligand showed stability after 60 ns (Supplementary Figure S6). Furthermore, each ligand showed acceptable RMSF values (< 3 Å) fit on the protein during 100 ns simulation, inferred the significant stability of docked bioactive compounds at the active site of jRdRp protein (Supplementary Figure S8).

Protein–ligand interaction profiling. The docked complexes of viral protein with potential compounds were also considered for protein–ligand interaction profiling against reference complex during the course of 100 ns simulation interval in terms of hydrogen bonding, hydrophobic interactions, ionic interactions, and water bridge formation (Fig. 5, Supplementary Figure S9-10).

In the case of jRdRp-Gedunin, docked complex exhibits hydrogen bond formation for 90% of the simulation time at Gly^{605} residue, Tyr^{610} and Trp^{800} residues noted for hydrophobic interactions for more than 50% of the simulation time, and Asp^{669} and Ser^{715} residues participated in water bridges for more than 30% of the MD time (Fig. 5a). Also, jRdRp-Nimbolide complex indicates hydrophobic interactions via Trp^{800} for 80% of the simulation time, Arg^{460} residue was noted for hydrogen bond formation in 30% of the simulation time, Arg^{474} and Ser^{604} residues contributed to water mediated interactions for 30% of the total simulation time (Fig. 5b). Moreover, jRdRp-Ohchinin complex exhibits the most stable hydrogen bond interaction at Arg^{474} with more than 100% of the simulation time and water bridges formation at Asp^{668} residue for 75% of the simulation interval (Fig. 5c). Furthermore, significant water bridge interactions via Arg^{484} (40%) and Asp^{668} (90%) were noted for the jRdRp-Kulactone docked complex during 100 ns simulation interval (Fig. 5d). However, reference complexes, viz. jRdRp-GTP and jRdRp-ATP, showed the most significant interaction at Arg^{474} via both hydrogen bonds and water bridge formation for 50% of the simulation interval (Supplementary Figure S11–12). Interestingly, the interactive residues were also observed in the respective docked complexes and essentially required for the replication of virus (Supplementary Table S2). Hence, these results support the considerable stability of selected compounds at the active pocket of jRdRp by formation of strong hydrogen bonding and hydrophobic interactions; hence, can be used as potent inhibitors of jRdRp protein.

Additionally, intermolecular interactions between the residues of jRdRp protein and potential bioactive compounds, i.e., Gedunin, Nimbolide, Ohchinin acetate, Kulactone, and reference ligands, viz. GTP and ATP, were calculated at total 30% interval of 100 ns simulation, which revealed considerable binding of respective ligands with active residues (Fig. 6, Supplementary Figure S8). Interestingly, all the selected ligands were observed for hydrogen bonding and water bridge interactions, suggested the stability of selected compounds at the active site of jRdRp protein. Hence, based on 100 ns molecular dynamics simulation analysis, docked complexes can be arranged in order of stability, i.e. jRdRp-Ohchinin acetate, jRdRp-Gedunin, jRdRp-Kulactone, and jRdRp-Nimbolide.

Binding free energy analysis. The binding affinities of the four selected protein–ligand complexes were estimated using MM/GBSA approach. Herein, poses of jRdRp-bioactive compounds, i.e., Gedunin, Nimbolide, Ohchinin acetate, and Kulactone, were extracted from 100 ns MD simulation trajectory at every 10 ns interval for average free binding energy calculations against reference complex, viz. jRdRP-GTP complex (Fig. 7, Supple-

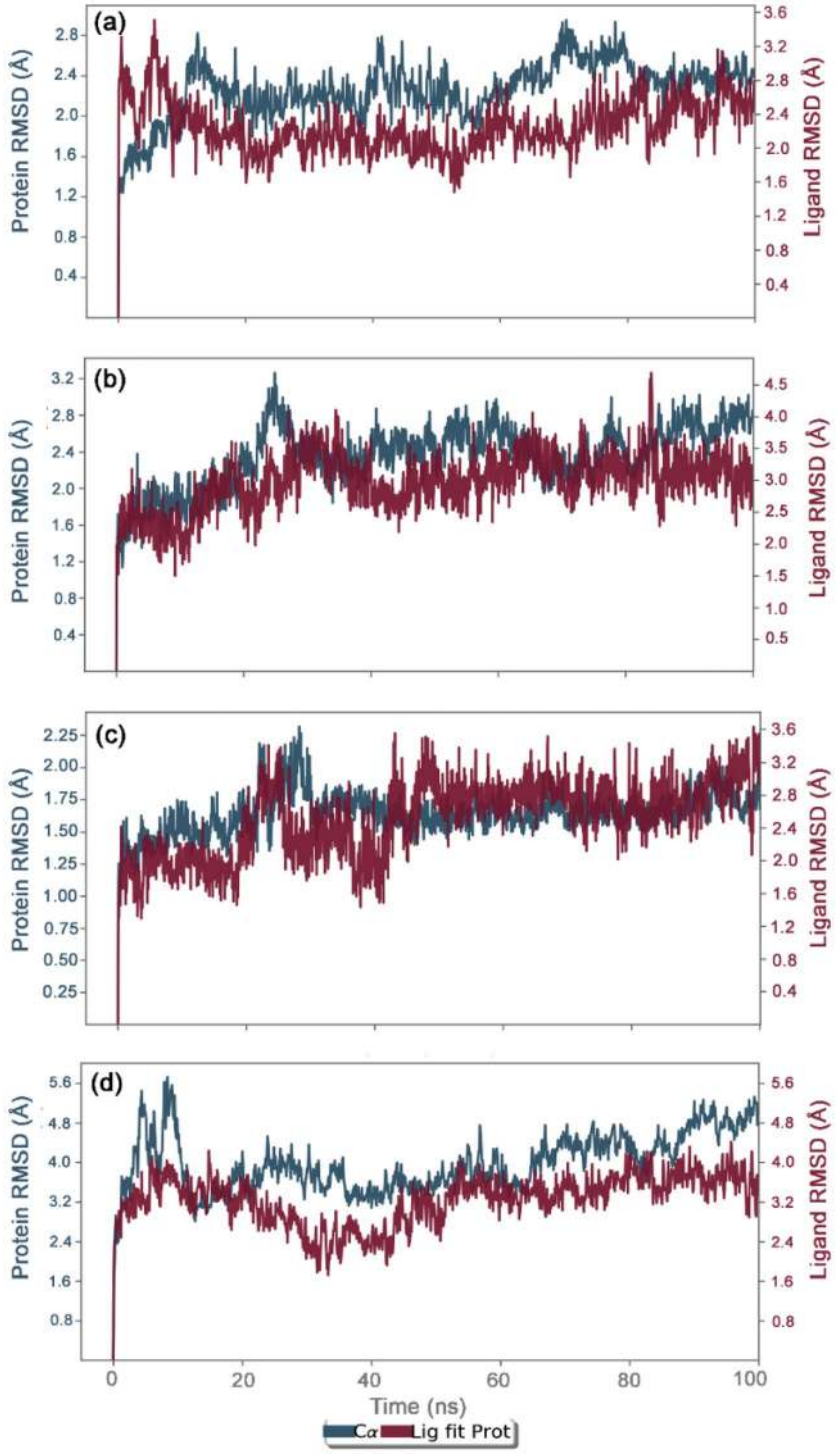

Figure 4. RMSD plots for the backbone atoms of jRdRp and selected bioactive compounds, i.e., (**a**) Gedunin (**b**) Nimbolide (**c**) Ohchinin acetate, (**d**) Kulactone fit on protein were extracted from 100 ns MD simulation trajectories of respective docked complexes.

mentary Table S4, Figure S9). All the docked complexes of bioactive compounds with jRdRp exhibits significant binding free energy (> − 50 kcal/mol). Of note, highest ΔG_{Bind} (− 61.13 ± 3.26 kcal/mol) was recorded for jRdRp-Nimbolide complex against jRdRp-GTP (ΔG_{Bind} = − 78.9 ± 9.05 kcal/mol) and jRdRp-ATP (− 33.34 ± 3.61 kcal/mol). Moreover, calculation of dissociation energy components for each complex exhibits substantial support of $\Delta G_{Bind\ Lipo}$, and $\Delta G_{Bind\ vdW}$ in the stability of docked complexes while $\Delta G_{Bind\ Solv\ GB}$ was observed in contribution for instability of the respective complexes (Fig. 7, Supplementary Figure S13). Conclusively, results suggested the

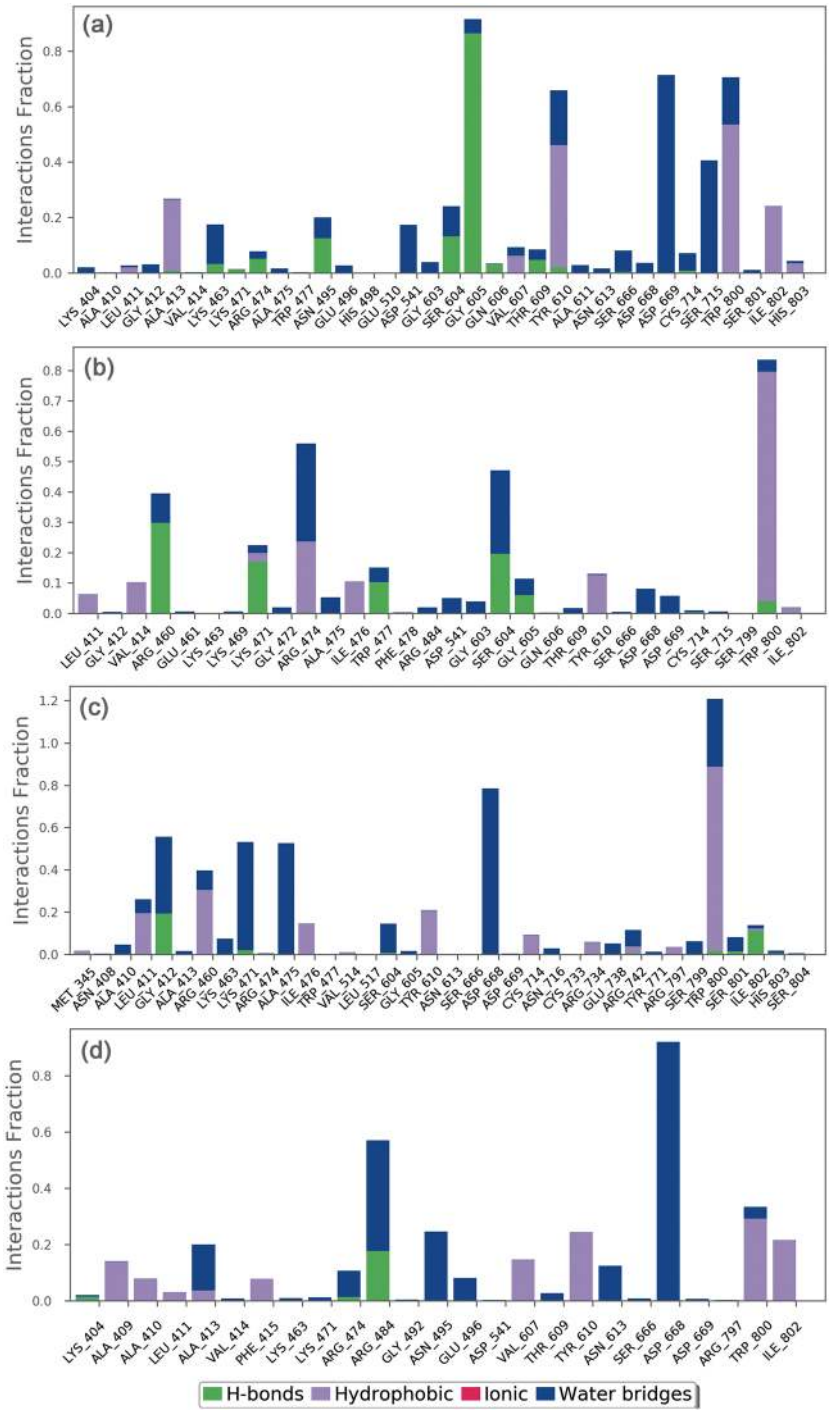

Figure 5. Protein–ligand interactions mapping for jRdRp docked with bioactive compounds, i.e., (**a**) Gedunin, (**b**) Nimbolide, (**c**) Ohchinin acetate, and (**d**) Kulactone, extracted from 100 ns MD simulations. Herein, values of interaction fractions > 1.0 are feasible as some residues established several interactions of the similar subtype.

considerable stability of docked bioactive compounds in via formation of van der Waals interactions with the essential residues in the active site of jRdRp protein.

Conclusion

The role of RNA dependent RNA polymerase (jRdRp) in the replication and survival of RNA genome viruses inside a host and absence of human homolog makes it an attractive molecular target for anti-viral drugs. Besides, board range of secondary metabolites as natural bioactive compounds in *Azadirachta indica* have been reported with medicinal benefits. Hence, this study evaluated the potential of known bioactive compounds in *Azadirachta*

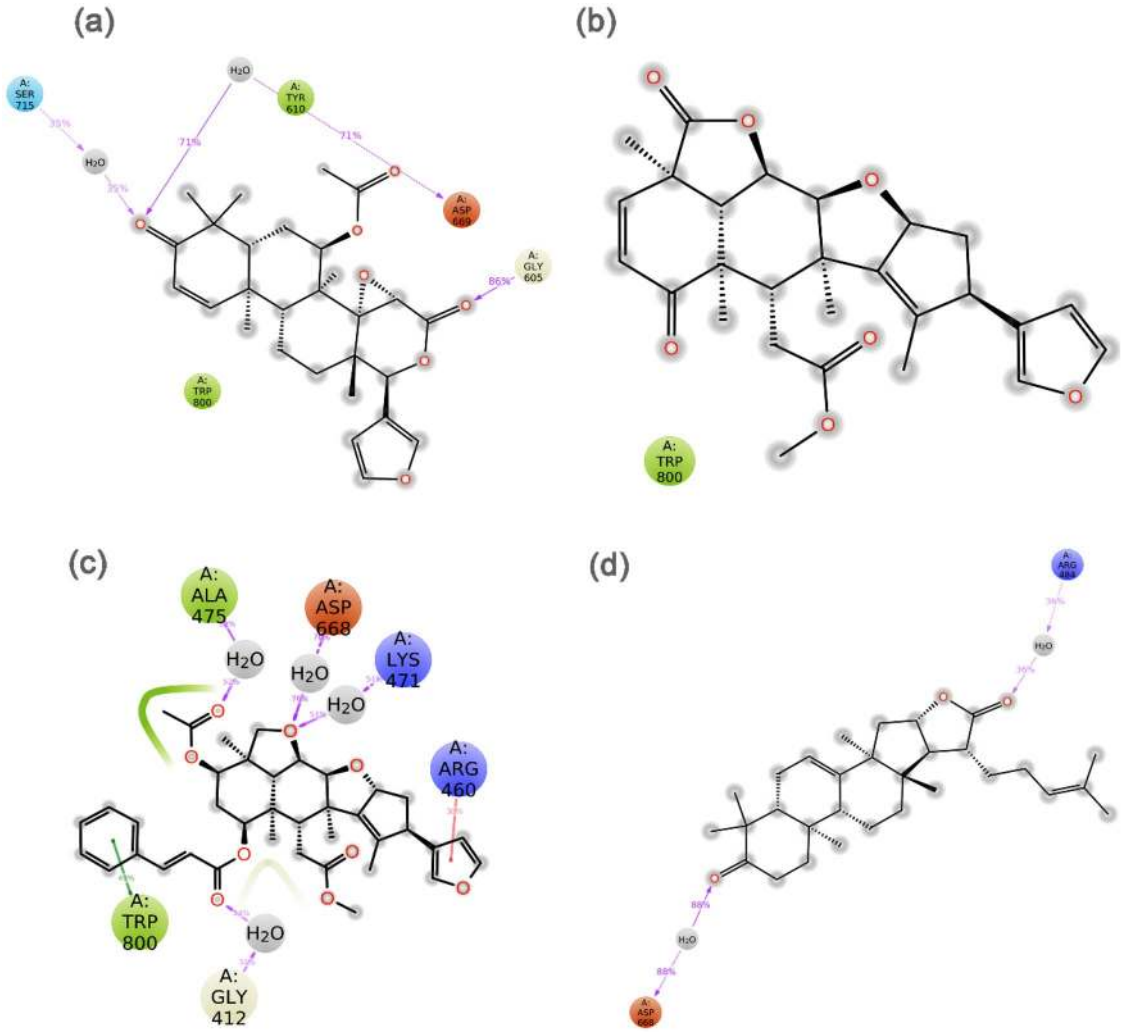

Figure 6. Schematic representation for interaction profile of jRdRp protein docked with bioactive compounds, i.e. (**a**) Gedunin, (**b**) Nimbolide, (**c**) Ohchinin acetate, and (**d**) Kulactone, extracted at 30% of total 100 ns simulation interval.

indica as potential inhibitors of jRdRp protein using complex molecular simulation, drug likeness profiling, and end-point binding free energy calculations. Herein, among the screened 43 bioactive compounds at the active site of jRdRp protein, four bioflavonoid compounds, viz. Gedunin, Nimbolide, Ohchinin acetate, and Kulactone, with substantial docking score and druglikeness were considered for further mechanistic inhibition analysis of jRdRp protein. The analysis of docked complexes showed that selected bioactive compounds occupied the active site by both hydrogen bonds, hydrophobic interactions, and other considerable intermolecular interactions with essential residues of jRdRp protein. Moreover, molecular dynamics simulation and free energy calculation further revealed the substantial stability and contribution of van der Waals interaction in the stability of respective docked complexes, respectively. The low penetration of the screened compounds to the BBB might affect their efficacy, however BBB penetration can be improved using SAR of the screened compounds during lead optimization. The investigated flavonoids might have potential effect against other flaviviruses which needs further investigation against specific viruses. In conclusion, these results supported the Gedunin, Nimbolide, Ohchinin acetate, and Kulactone as acceptable inhibitors of jRdRp protein and advised to studied for further in vitro and in vivo experiments to develop potential treatment against Japanese encephalitis virus.

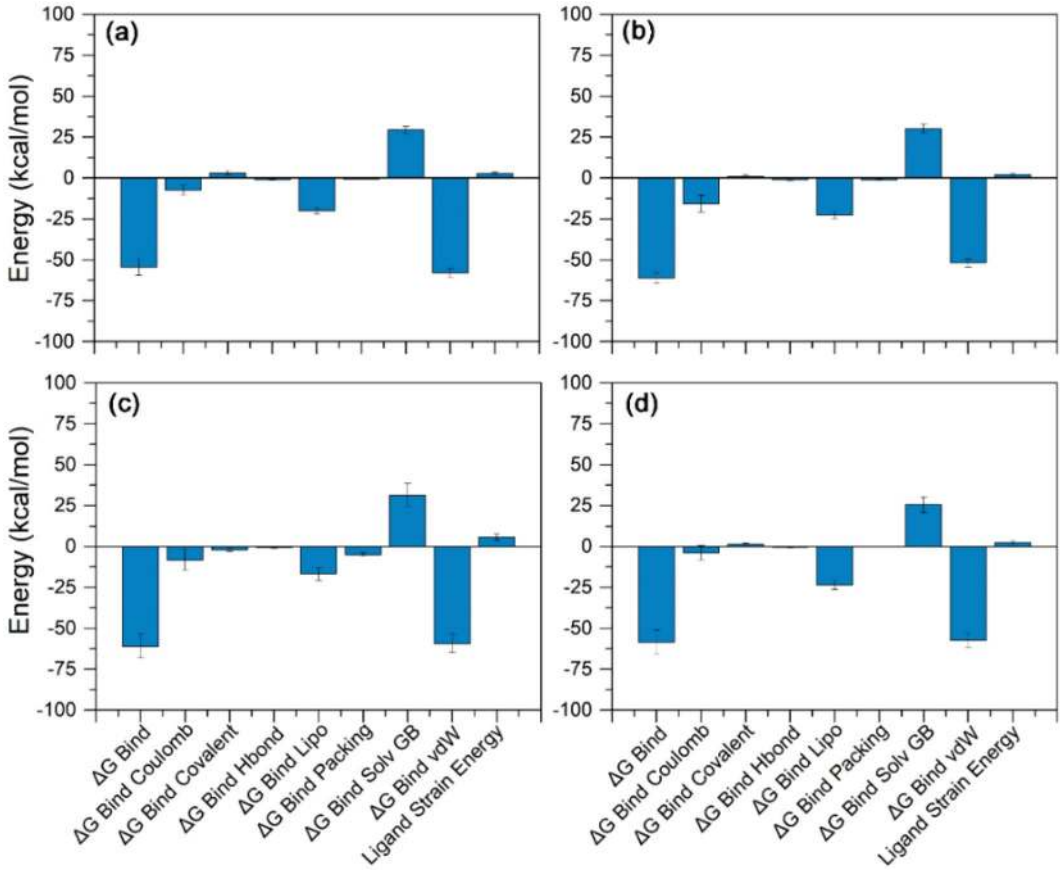

Figure 7. Binding free energy and individual dissociation energy components calculation performed for jRdRp protein docked with bioactive compounds, i.e. (**a**) Gedunin, (**b**) Nimbolide, (**c**) Ohchinin acetate, and (**d**) Kulactone, on the extracted poses from total 100 ns simulation interval.

Received: 7 June 2021; Accepted: 18 August 2021
Published online: 13 September 2021

References

1. Zhou, X. *et al.* Inhibition of Japanese encephalitis virus proliferation by long non-coding RNA SUSAJ1 in PK-15 cells. *Virol. J.* **18**, 29. https://doi.org/10.1186/s12985-021-01492-5 (2021).
2. Turtle, L. & Solomon, T. Japanese encephalitis—the prospects for new treatments. *Nat. Rev. Neurol.* **14**, 298–313. https://doi.org/10.1038/nrneurol.2018.30 (2018).
3. Tu, T. *et al.* Association between meteorological factors and the prevalence dynamics of Japanese encephalitis. *PLoS One* **16**, e0247980. https://doi.org/10.1371/journal.pone.0247980 (2021).
4. Campbell, G. L. *et al.* Estimated global incidence of Japanese encephalitis: A systematic review. *Bull. World Health Organ.* **89**(766–774), 774A-774E. https://doi.org/10.2471/BLT.10.085233 (2011).
5. Wang, H. & Liang, G. Epidemiology of Japanese encephalitis: Past, present, and future prospects. *Ther. Clin. Risk Manag.* **11**, 435–448. https://doi.org/10.2147/TCRM.S51168 (2015).
6. Hills, S. L. & Phillips, D. C. Past, present, and future of Japanese encephalitis. *Emerg. Infect. Dis.* **15**, 1333. https://doi.org/10.3201/eid1508.090149 (2009).
7. Mathers, C. D., Ezzati, M. & Lopez, A. D. Measuring the burden of neglected tropical diseases: The global burden of disease framework. *PLoS Negl. Trop. Dis.* **1**, e114. https://doi.org/10.1371/journal.pntd.0000114 (2007).
8. Kumar, P., Pisudde, P. M., Sarthi, P. P., Sharma, M. P. & Keshri, V. R. Status and trend of acute encephalitis syndrome and Japanese encephalitis in Bihar, India. *Natl. Med. J. India* **30**, 317–320. https://doi.org/10.4103/0970-258X.239070 (2017).
9. Kim, Y. G., Yoo, J. S., Kim, J. H., Kim, C. M. & Oh, J. W. Biochemical characterization of a recombinant Japanese encephalitis virus RNA-dependent RNA polymerase. *BMC Mol. Biol.* **8**, 59. https://doi.org/10.1186/1471-2199-8-59 (2007).
10. Sumiyoshi, H. *et al.* Complete nucleotide sequence of the Japanese encephalitis virus genome RNA. *Virology* **161**, 497–510. https://doi.org/10.1016/0042-6822(87)90144-9 (1987).
11. Bhardwaj, T. *et al.* Japanese encephalitis virus - exploring the dark proteome and disorder-function paradigm. *FEBS J.* **287**, 3751–3776. https://doi.org/10.1111/febs.15427 (2020).
12. Chambers, T. J., Hahn, C. S., Galler, R. & Rice, C. M. Flavivirus genome organization, expression, and replication. *Annu. Rev. Microbiol.* **44**, 649–688. https://doi.org/10.1146/annurev.mi.44.100190.003245 (1990).
13. Fernandez-Garcia, M. D., Mazzon, M., Jacobs, M. & Amara, A. Pathogenesis of flavivirus infections: Using and abusing the host cell. *Cell Host Microbe* **5**, 318–328. https://doi.org/10.1016/j.chom.2009.04.001 (2009).
14. Laureti, M., Narayanan, D., Rodriguez-Andres, J., Fazakerley, J. K. & Kedzierski, L. Flavivirus receptors: Diversity, identity, and cell entry. *Front. Immunol.* **9**, 2180. https://doi.org/10.3389/fimmu.2018.02180 (2018).

15. Smit, J. M., Moesker, B., Rodenhuis-Zybert, I. & Wilschut, J. Flavivirus cell entry and membrane fusion. *Viruses* **3**, 160–171. https://doi.org/10.3390/v3020160 (2011).
16. Solomon, T. *et al.* Origin and evolution of Japanese encephalitis virus in southeast Asia. *J. Virol.* **77**, 3091–3098. https://doi.org/10.1128/jvi.77.5.3091-3098.2003 (2003).
17. Malet, H. *et al.* Crystal structure of the RNA polymerase domain of the West Nile virus non-structural protein 5. *J. Biol. Chem.* **282**, 10678–10689. https://doi.org/10.1074/jbc.M607273200 (2007).
18. O'Reilly, E. K. & Kao, C. C. Analysis of RNA-dependent RNA polymerase structure and function as guided by known polymerase structures and computer predictions of secondary structure. *Virology* **252**, 287–303. https://doi.org/10.1006/viro.1998.9463 (1998).
19. Behrens, S. E., Tomei, L. & De Francesco, R. Identification and properties of the RNA-dependent RNA polymerase of hepatitis C virus. *EMBO J* **15**, 12–22 (1996).
20. Mackenzie, J. M., Jones, M. K. & Westaway, E. G. Markers for trans-Golgi membranes and the intermediate compartment localize to induced membranes with distinct replication functions in flavivirus-infected cells. *J. Virol.* **73**, 9555–9567. https://doi.org/10.1128/JVI.73.11.9555-9567.1999 (1999).
21. Filgueira, L. & Lannes, N. Review of emerging Japanese encephalitis virus: New aspects and concepts about entry into the brain and inter-cellular spreading. *Pathogens* https://doi.org/10.3390/pathogens8030111 (2019).
22. Kalia, M., Khasa, R., Sharma, M., Nain, M. & Vrati, S. Japanese encephalitis virus infects neuronal cells through a clathrin-independent endocytic mechanism. *J. Virol.* **87**, 148–162. https://doi.org/10.1128/Jvi.01399-12 (2013).
23. Johnston, L. J., Halliday, G. M. & King, N. J. Langerhans cells migrate to local lymph nodes following cutaneous infection with an arbovirus. *J. Invest. Dermatol.* **114**, 560–568. https://doi.org/10.1046/j.1523-1747.2000.00904.x (2000).
24. Sengupta, N. & Basu, A. Japanese encephalitis virus infection: Effect on brain development and repair. *Curr. Sci. India* **105**, 815–820 (2013).
25. Maximova, O. A. & Pletnev, A. G. Flaviviruses and the central nervous system: Revisiting neuropathological concepts. *Annu. Rev. Virol.* **5**, 255–272. https://doi.org/10.1146/annurev-virology-092917-043439 (2018).
26. Johansen, C. A. *et al.* Entomological investigations of an outbreak of Japanese encephalitis virus in the Torres Strait, Australia, in 1998. *J. Med. Entomol.* **38**, 581–588. https://doi.org/10.1603/0022-2585-38.4.581 (2001).
27. Halstead, S. B. & Jacobson, J. Japanese encephalitis. *Adv. Virus Res.* **61**, 103–138 (2003).
28. Ghosh, D. & Basu, A. Japanese encephalitis—a pathological and clinical perspective. *PLoS Negl. Trop. Dis.* **3**, e437. https://doi.org/10.1371/journal.pntd.0000437 (2009).
29. Wu, S. F. *et al.* Antiviral effects of an iminosugar derivative on flavivirus infections. *J. Virol.* **76**, 3596–3604. https://doi.org/10.1128/jvi.76.8.3596-3604.2002 (2002).
30. Chang, C. C., Ou, Y. C., Raung, S. L. & Chen, C. J. Antiviral effect of dehydroepiandrosterone on Japanese encephalitis virus infection. *J. Gen. Virol.* **86**, 2513–2523. https://doi.org/10.1099/vir.0.81123-0 (2005).
31. Sebastian, L. *et al.* N-methylisatin-beta-thiosemicarbazone derivative (SCH 16) is an inhibitor of Japanese encephalitis virus infection in vitro and in vivo. *Virol. J.* https://doi.org/10.1186/1743-422x-5-64 (2008).
32. Chang, S. J., Chang, Y. C., Lu, K. Z., Tsou, Y. Y. & Lin, C. W. Antiviral activity of isatis indigotica extract and its derived indirubin against Japanese encephalitis virus. *Evid. Based Complement Alternat. Med.* **2012**, 925830. https://doi.org/10.1155/2012/925830 (2012).
33. Wang, S. *et al.* Screening of FDA-approved drugs for inhibitors of Japanese encephalitis virus infection. *J. Virol.* https://doi.org/10.1128/JVI.01055-17 (2017).
34. Nawa, M., Takasaki, T., Yamada, K. I., Kurane, I. & Akatsuka, T. Interference in Japanese encephalitis virus infection of Vero cells by a cationic amphiphilic drug, chlorpromazine. *J. Gen. Virol.* **84**, 1737–1741. https://doi.org/10.1099/vir.0.18883-0 (2003).
35. Ye, J. *et al.* Etanercept reduces neuroinflammation and lethality in mouse model of Japanese encephalitis. *J. Infect. Dis.* **210**, 875–889. https://doi.org/10.1093/infdis/jiu179 (2014).
36. Mishra, M. K. & Basu, A. Minocycline neuroprotects, reduces microglial activation, inhibits caspase 3 induction, and viral replication following Japanese encephalitis. *J. Neurochem.* **105**, 1582–1595. https://doi.org/10.1111/j.1471-4159.2008.05238.x (2008).
37. Guo, J. *et al.* Screening of natural extracts for inhibitors against Japanese encephalitis virus infection. *Antimicrob. Agents Chemother.* https://doi.org/10.1128/AAC.02373-19 (2020).
38. Braga, T. M. *et al. Azadirachta indica*. A juss in vivo toxicity—an updated review. *Molecules* **26**, 252 (2021).
39. Biswas, K., Chattopadhyay, I., Banerjee, R. K. & Bandyopadhyay, U. Biological activities and medicinal properties of neem (*Azadirachta indica*). *Curr. Sci. India* **20**, 1336–1345 (2002).
40. Parida, M. M., Upadhyay, C., Pandya, G. & Jana, A. M. Inhibitory potential of neem (*Azadirachta indica* Juss) leaves on dengue virus type-2 replication. *J. Ethnopharmacol.* **79**, 273–278. https://doi.org/10.1016/s0378-8741(01)00395-6 (2002).
41. Atawodi, S. E. & Atawodi, J. C. *Azadirachta indica* (neem): A plant of multiple biological and pharmacological activities. *Phytochem. Rev.* **8**, 601–620. https://doi.org/10.1007/s11101-009-9144-6 (2009).
42. Subapriya, R. & Nagini, S. Medicinal properties of neem leaves: A review. *Curr. Med. Chem. Anticancer Agents* **5**, 149–146. https://doi.org/10.2174/1568011053174828 (2005).
43. Dwivedi, V. D. *et al.* Anti-dengue infectivity evaluation of bioflavonoid from *Azadirachta indica* by dengue virus serine protease inhibition. *J. Biomol. Struct. Dyn.* **39**, 1417–1430. https://doi.org/10.1080/07391102.2020.1734485 (2021).
44. Surana, P., Satchidanandam, V. & Nair, D. T. RNA-dependent RNA polymerase of Japanese encephalitis virus binds the initiator nucleotide GTP to form a mechanistically important pre-initiation state. *Nucleic Acids Res.* **42**, 2758–2773. https://doi.org/10.1093/nar/gkt1106 (2014).
45. Labbe, C. M. *et al.* MTiOpenScreen: A web server for structure-based virtual screening. *Nucleic Acids Res.* **43**, W448-454. https://doi.org/10.1093/nar/gkv306 (2015).
46. Kim, S. *et al.* PubChem in 2021: New data content and improved web interfaces. *Nucleic Acids Res.* **49**, D1388–D1395. https://doi.org/10.1093/nar/gkaa971 (2021).
47. Pettersen, E. F. *et al.* UCSF Chimera—a visualization system for exploratory research and analysis. *J. Comput. Chem.* **25**, 1605–1612. https://doi.org/10.1002/jcc.20084 (2004).
48. Daina, A., Michielin, O. & Zoete, V. SwissADME: A free web tool to evaluate pharmacokinetics, drug-likeness and medicinal chemistry friendliness of small molecules. *Sci. Rep.* **7**, 42717. https://doi.org/10.1038/srep42717 (2017).
49. Cheng, F. *et al.* Correction to "admetSAR: A comprehensive source and free tool for assessment of chemical ADMET properties". *J. Chem. Inf. Model.* **59**, 4959. https://doi.org/10.1021/acs.jcim.9b00969 (2019).
50. Bharadwaj, S., Lee, K. E., Dwivedi, V. D. & Kang, S. G. Computational insights into tetracyclines as inhibitors against SARS-CoV-2 M-pro via combinatorial molecular simulation calculations. *Life Sci.* https://doi.org/10.1016/j.lfs.2020.118080 (2020).
51. Trott, O. & Olson, A. J. AutoDock Vina: Improving the speed and accuracy of docking with a new scoring function, efficient optimization, and multithreading. *J. Comput. Chem.* **31**, 455–461. https://doi.org/10.1002/jcc.21334 (2010).
52. Kevin J. Bowers, *et al.* Scalable Algorithms for Molecular Dynamics Simulations on Commodity Clusters, Proceedings of the ACM/IEEE Conference on Supercomputing (SC06), Tampa, Florida, November 11–17, 2006 .
53. Bharadwaj, S. *et al.* Density functional theory and molecular dynamics simulation support *Ganoderma lucidum* triterpenoids as broad range antagonist of matrix metalloproteinases. *J. Mol. Liq.* https://doi.org/10.1016/j.molliq.2020.113322 (2020).
54. Macarron, R. Critical review of the role of HTS in drug discovery. *Drug Discov. Today* **11**, 277–279. https://doi.org/10.1016/j.drudis.2006.02.001 (2006).

55. Lipinski, C. A. Lead- and drug-like compounds: The rule-of-five revolution. *Drug Discov. Today Technol.* **1**, 337–341. https://doi.org/10.1016/j.ddtec.2004.11.007 (2004).
56. Bharadwaj, S., Lee, K. E., Dwivedi, V. D. *et al.* Discovery of Ganoderma lucidum triterpenoids as potential inhibitors against Dengue virus NS2B-NS3 protease. Sci Rep **9**, 19059. https://doi.org/10.1038/s41598-019-55723-5 (2019).
57. Bharadwaj, S., Kumar Rao, A., Dwivedi, V. D., Mishra, S. K., & Yadava, U. Structure-based screening and validation of bioactive compounds as Zika virus methyltransferase (MTase) inhibitors through first-principle density functional theory, classical molecular simulation and QM/MM affinity estimation. *J Biomolecul Str and Dynamics*, **39**(7), 2338–2351, https://doi.org/10.1080/07391102.2020.1747545 (2021).

Acknowledgements

Author, Ankita Singh acknowledge the Director, AIRF, Jawaharlal Nehru University, New Delhi, India for giving access to Schrödinger program. The authors acknowledge the generous charitable donation from the late Sheikh Ibraheem Ahmed Azhar as a contribution to the scientific research community.

Author contributions

Conceptualization, V.D.D and A.S., methodology, V.D.D, A.S., T.A.A, and A.A.F.; formal analysis, S.A.E.-K., V.D.D and A.S. investigation,V.D.D., A.S., L.H.B., T.A.A,and S.A.E.-K. data curation, V.D.D., E.I.A., M.A.K., and A.S.; writing—original draft preparation, V.D.D., A.S., S.A.E.-K., M.A.K., and E.I.A.; writing—review and editing, All authors; supervision, M.A.K., and E.I.A.; project administration, E.I.A All authors have read and agreed to the published version of the manuscript.

Competing interests

The authors declare no competing interests.

Additional information

Supplementary Information The online version contains supplementary material available at https://doi.org/10.1038/s41598-021-96917-0.

Correspondence and requests for materials should be addressed to E.I.A.

Reprints and permissions information is available at www.nature.com/reprints.

Publisher's note Springer Nature remains neutral with regard to jurisdictional claims in published maps and institutional affiliations.